Charge Density Study of Naphthalene Based on X-ray Diffraction Data at Four Different Temperatures and Theoretical Calculations

Jette Oddershede and Sine Larsen*

Centre for Crystallographic Studies, Department of Chemistry, University of Copenhagen, Universitetsparken 5, DK-2100 Copenhagen Ø, Denmark

Received: July 26, 2003; In Final Form: November 24, 2003

The crystal electron density of naphthalene has been investigated on the basis of highly redundant X-ray diffraction data collected to high resolution at 100, 135, 170, and 205 K and from quantum chemical calculations. An analysis of the X-ray diffraction data showed that for the data collected below 200 K thermal motion can be successfully deconvoluted from the diffraction data. A topological analysis of the resulting static crystal electron-density map revealed that the intramolecular bond critical points have characteristics that are very similar to those of the isolated molecule. There is excellent agreement between the bond critical points corresponding to the intermolecular interactions in the experimental and theoretical crystal electron densities. The strongest intermolecular interaction is a C−H···π interaction that causes a change in the electron distribution of the C−H bond.

Introduction

The topological analysis of the electron density derived from theoretical calculations as devised by R. F. W. Bader[1] has proven to be a useful tool in obtaining valuable information about chemical bonding and the properties of atoms in molecules. The topological analysis has recently been extended to experimental electron densities obtained by X-ray diffraction.[2] The X-ray diffraction experiment provides information on the electron density averaged over the thermal motions in the crystal at the given temperature. Therefore, it is necessary to deconvolute the thermal motion of the atoms to obtain the static electron density, which can be subjected to a topological analysis and compared to results from theoretical calculations. Considering the growth in the topological analysis based on experimental charge densities, we found it timely to investigate to which degree it is possible to deconvolute the thermal motion from the experimental electron density to provide a reliable static electron density from an X-ray diffraction experiment. If the thermal motion has been successfully deconvoluted, then one should obtain identical atomic multipole parameters from refinements of accurate, high-order X-ray diffraction data irrespective of the temperature. To examine whether this is possible, we undertook a study of the charge density of naphthalene at multiple temperatures.

Naphthalene, which crystallizes in the monoclinic space group $P2_1/c$ with the molecule on a crystallographic inversion center, was an obvious choice for an investigation of this type. Its crystal structure and thermal motion have been investigated previously from X-ray[3−6] and neutron[7,8] diffraction data. The more recent studies of thermal motion in crystalline naphthalene from X-ray diffraction experiments are all based on the X-ray diffraction data reported by Brock and Dunitz[6] in 1982. They collected five data sets at temperatures between 92 and 239 K to a maximum resolution in $\sin\theta/\lambda$ of 0.65 Å^{-1} (Mo Kα). The availability of area detectors has led to a significant reduction of the time required to measure data for a charge density study, making it possible to collect accurate, high-resolution data at several temperatures for charge density studies of naphthalene within a reasonable time frame.

In their original work, Brock and Dunitz employed atomic scattering factors corresponding to independent, spherical atoms, and the thermal motion was modeled by anisotropic displacement parameters (ADP) for the carbon atoms and isotropic displacement parameters for the hydrogen atoms. The refined ADPs were used in a rigid body (**TLS**) analysis,[9] where the effects of subtracting the contributions from internal vibrations before the determination of the rigid body parameters were analyzed. This analysis was compared to lattice dynamical calculations. Brock, Dunitz, and Hirshfeld (BDH)[10] used the same data later in a refinement that employed the multipole parameters obtained from a high-resolution study of the related hydrocarbon perylene. In this work, the rigid body tensors **T** and **L** (**S** is vanishing because of the molecular inversion center) were refined directly from the data, and the final ADPs were obtained after adding the contributions from internal vibrations. The latest reported study of the thermal motion in crystalline naphthalene was, to our knowledge, carried out by Bürgi, Rangavittal, and Hauser in 2001.[11] They analyzed the ADPs obtained from the BDH rerefinement using an Einstein-type model of local molecular normal modes.

Our analysis of X-ray diffraction data sets measured for naphthalene at 100, 135, 170, and 205 K showed that the deconvolution of the thermal motions was achieved, which gives us faith in the experimentally determined crystal electron density. To have an independent measure of the derived static electron densities, quantum chemical calculations were conducted to determine the electron density for the periodic crystal and an isolated molecule. As an unexpected bonus, the subsequent topological analysis of the theoretical and experimental electron densities revealed new interesting features of the intermolecular interactions.

* Corresponding author. Present address: European Synchrotron Radiation Facility B. P. 220, F-38043 Grenoble Cedex, France. Telephone: (+33) (0)4 7688 2181. Fax: (+33) (0)4 7688 2060. E-mail: slarsen@esrf.fr.

10.1021/jp036186g CCC: $27.50
Published on Web 01/20/2004

TABLE 1: Data Collection and Reduction

	100 K	135 K 135a K	170 K 170a K	205 K[a] 205a K
a/Å	7.8248(2)	7.8596(1)	7.8930(1)	7.9410(1)
		7.8612(1)	7.8926(1)	7.9435(1)
b/Å	5.9349(1)	5.9383(1)	5.9443(1)	5.9528(1)
		5.9413(1)	5.9426(1)	5.9534(1)
c/Å	8.0997(2)	8.1204(1)	8.1413(1)	8.1656(1)
		8.1224(1)	8.1383(1)	8.1645(1)
β/deg	114.441(2)	114.634(1)	114.803(1)	115.101(1)
		114.528(1)	114.764(1)	114.998(1)
V/Å^3	342.44(1)	344.50(1)	346.74(1)	349.54(1)
		345.13(1)	346.61(1)	349.93(1)
$(\sin\theta/\lambda)_{max}$/Å^{-1}	1.15	1.16	1.17	
		1.14	1.14	1.13
total refl	58 839	62 766	63 685	
		63 703	63 630	63 300
R_{int}	0.0305	0.0446	0.0406	
		0.0274	0.0304	0.0321
unique refl	4368	4515	4673	
		4288	4302	4250

[a] Incomplete data set.

TABLE 2: Final Residuals from the Refinements[a]

	R1	wR2	GOF	$\lvert\Delta\rho\rvert_{max}$/eÅ^{-3} [b]
100 K	0.0177	0.0261	0.9217	0.11
135a K	0.0203	0.0281	0.9269	0.13
170a K	0.0287	0.0339	0.9959	0.15
205a K	0.0373	0.0364	0.9519	0.13

[a] Experimental weights, $w = 1/(\sigma^2(|F|^2))$. [b] 0.02-Å grid.

Experimental Section

Naphthalene crystals suitable for X-ray diffraction experiments were grown from an ethanol solution (0.1 g of naphthalene in 3 mL of ethanol) at room temperature (25 °C). The crystals sublimed quickly if left uncovered at room temperature but could be kept in closed containers at 5 °C for several months.

Data Collection. Data were collected with a Nonius KappaCCD instrument[12] using graphite-monochromated Mo Kα radiation. An Oxford Cryo Systems AD41 was used to maintain the desired temperature during data collection. The data-collection temperatures were determined in the following way: An exhaust temperature of 116.0 K was shown to correspond to 122.4 K at the crystal mounting position (calibrated on the basis of the phase transition of KH_2PO_4),[13] and a linear interpolation was carried out assuming that this temperature difference had vanished at 295 K (the temperature of the diffractometer room).

A crystal of approximately $0.4 \times 0.4 \times 0.3$ mm^3 was encased in epoxy glue to prevent sublimation during data collection[6] and was immediately mounted on the diffractometer at 100 K. Unfortunately, the epoxy glue reacted with the crystal, resulting in an increase in low-angle powder lines during the data collection, so only the data sets 100 K, 135 K, and 170 K and parts of set 205 K were collected on this crystal. Another crystal of $0.45 \times 0.4 \times 0.35$ mm^3 was chosen and coated with baby oil. Because data sets 135 K and 170 K from the previous crystal merged poorly (Table 1), data at these temperatures were measured again; thus data sets 135a K, 170a K, and 205a K were collected on the second crystal.

In accordance with the data-collection strategy of Sørensen and Larsen,[14] the data collections were split into three θ ranges: 20−57, 1−40, and 1−25°. To prevent the overflow of the detector, the three θ intervals were collected using scan times of 300, 150, and 15 s/deg, respectively. Furthermore, it was necessary to reduce the generator setting of the 1−25° range. The intensity decay during the exposure time (9 days per data set) was monitored by intermediate ϕ scans approximately every second day, collecting each time a total of 13 frames corresponding to around 80 reflections in the θ range of 7−25°.

The cell dimensions (Table 1) were determined from the about 400 frames in the second scan set of each data collection using DirAx,[15] which gave 200−250 reflections in the θ range of 15−50°. The lattice parameters display the same temperature dependence as observed in the multi-temperature study of Brock and Dunitz,[6] but our results are systematically 0.2% lower. The resulting difference in unit cell volume could reflect a discrepancy between the temperature scales of the two studies, corresponding to a ΔT of around 30 K.

Data Reduction. Data collected at different generator settings were processed separately using EvalCCD.[16] All reflections were corrected for background, Lorentz, and polarization effects. With the size of the crystals and $\mu = 0.070(1)$ mm^{-1}, absorption effects were considered to be negligible ($T_{min} = 0.970$, $T_{max} = 0.979$). The average intensity decay observed for each data set was less than half of $\sigma(I)$, so no corrections for intensity changes during exposure time were judged necessary. The program SORTAV was used to scale and average the data.[17] Only reflections with $I \geq 10\sigma(I)$ were used to determine the intersubset scale factors. No reflections were rejected, and a $\sin\theta/\lambda$ cutoff corresponding to a completeness larger than 95% in the utmost shell was applied.

Least-Squares Refinements. Least-squares minimizations of $\sum w(|F_o|^2 - |F_c|^2)^2$ using all reflections were carried out with the program VALRAY,[18] which was also used for the topological analysis of the experimental static electron densities. The poor merging statistics of data sets 135 K and 170 K made us exclude these from the refinements, thus refinements were carried out for only the following data sets: 100 K, 135a K, 170a K, and 205a K.

The generalized X-ray scattering factor model[19] was used to describe the atoms in the present study. According to a similar study of the electron density in crystalline benzene,[20] the positional and thermal parameters for the hydrogen atoms can be obtained from two sets of neutron diffraction data collected above and below the temperature interval of the X-ray study. Neutron diffraction studies have been carried out for naphthalene at 12 K[8] and 295 K;[7] however, it is obvious that the two data sets are not of the same accuracy as those used in the analysis of benzene. This is most pronounced for the data measured at 295 K, in which the ADPs were obtained by the use of a rigid body thermal parameter constraint to reduce the number of variables in the refinement. We concluded that the thermal parameters that could be obtained on the basis of these results would be unreliable, and the same applies to the positional parameters because of the large difference in temperature.

Instead we used the procedure by Madsen et al.[21] to obtain the positional and thermal parameters for the hydrogen atoms. A refinement was carried out that modeled the carbon atoms freely (refining positions, ADPs, multipoles up to the octopole level, and radial parameters) as well as positional and isotropic displacement parameters for the hydrogen atoms. The resulting C−H bonds were then elongated to 1.083 Å, the standard neutron distance for aromatic C−H bonds. The hydrogen atoms were fixed at these positions for the subsequent refinements.

After a second round of refinements, the ADPs of the carbon atoms were used as input for a rigid body analysis to determine the rigid body translational and librational tensors, **T** and **L** (Table 2S), by a least-squares fit with the program THMA11.[22]

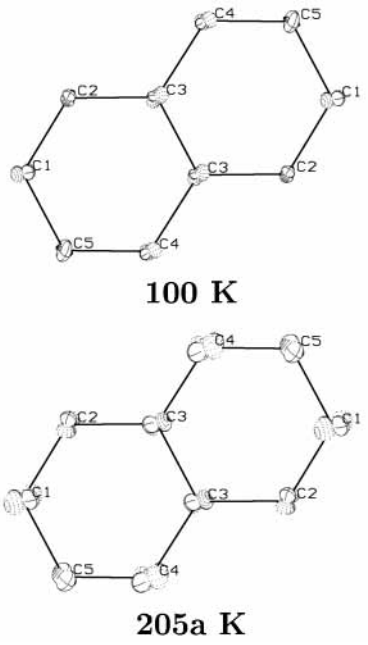

Figure 1. Differences between the observed ADPs of the carbon atoms and those obtained from the rigid body model illustrated by PEANUT[24] plots. The scale is 12.32, 8 times larger than the one used in Figure 2.

Figure 1 is an illustration of the difference between the observed ADPs and those obtained from the **T** and **L** tensors. The rigid body model describes the ADPs well, and similar differences corresponding to the internal vibrations are seen at the two temperature extremes. The contribution from the internal vibrations of the carbon atoms was not subtracted from the observed ADPs prior to the rigid body analysis and could therefore influence the obtained **T** and **L** tensors. To estimate the discrepancy between the **T** and **L** tensors obtained from the raw ADPs and those from the ADPs corrected for internal vibrations, we used the results from the theoretical calculations (see below) to obtain the contributions from the internal vibrations to be subtracted from the raw ADPs at 100 and 205 K. The differences between the first set of **T** and **L** and these more correct rigid body tensors are within 10%. A recent analysis based on several neutron data sets has shown that a rigid body on the raw ADPs gives a good estimate of the rigid body contributions to the ADPs of the hydrogen atoms.[23] Taking these results into account, we found that correcting the ADPs did not provide sufficient improvement of the **T** and **L** tensors obtained from the uncorrected ADPs.

The ADPs used for the hydrogen atoms in the final refinements were thus obtained from the uncorrected rigid body parameters with the addition of the contributions from internal vibrations. On the basis of tabulated vibrational frequencies for aromatic molecules and our experiences from previous work,[21] the contributions from internal vibrations were estimated to be 0.005 Å^2 along the C−H bond and 0.01 Å^2 in the two perpendicular directions (both in-plane and out-of-plane). The deviations between these very rough estimates and the internal vibrations from the DFT calculations are around 10%. Modeling the hydrogen atoms up to the quadrupole level including radial parameters, we refined a total of 165 parameters leading to the residuals listed in Table 2.

Theoretical Calculations

Periodic Calculation of the Crystal Electron Density. A single-point periodic calculation based on the 135a K experimental geometry was performed with the program CRYSTAL98[25] at the B3LYP[26,27] level using the 6-31G** basis set[28] (30 K-points in the irreducible Brillouin zone, ITOL1 = ITOL2 = ITOL3 = ITOL4 = 6, ITOL5 = 14). No scaling of the exponents of the polarization functions was performed because of the large difference between the integral truncation parameters ITOL4 and ITOL5.[29] Exponents of nonpolarization functions on the hydrogen atoms were scaled by a factor of 1.1. The topological analysis of the electron density was performed using TOPOND98.[30]

Isolated-Molecule Geometry Optimization and Frequency Calculation. Geometry optimization of a naphthalene molecule with D_{2h} symmetry (five independent atoms (C(1), C(2), C(3), H(1), and H(2); see Figure 2) was performed with the program Gaussian 94[31] at the B3LYP/6-31G** level. A frequency calculation for the geometry-optimized molecule was subsequently performed at the same level of theory. The AIMPAC package[32] was used for the topological analysis of the electron density.

Results and Discussion

Deconvolution of Thermal Motion from Electron Density. In the comparative analysis of the static electron densities derived from the multipole refinements, we paid close attention to the following features: The model must show good agreement between observed and calculated structure factors (i.e., a low R factor). There is also the demand for a flat and featureless difference electron density map, $\Delta\rho = \rho_{obs} - \rho_{calc}$. Furthermore, the electron density should be described solely by the atomic scattering factors, and the thermal motion, by the ADPs. This implies that the atomic multipole parameters should be temperature-independent.

The difference density maps calculated from the applied model using all data to maximum resolution are flat (±0.15 eÅ^{-3}, Table 2), and a comparison of maps obtained at different temperatures shows no coinciding peak features (Figure 1S). Furthermore, the R values are low. The ORTEP[33] plots of Figure 2 show the thermal ellipsoids increasing in size with increasing temperature. It is noteworthy that the principal axes for all atoms maintain their orientations in the four refinements.

We have investigated the similarity of the atomic electronic parameters by calculating the distance in parameter space between the parameters obtained from refinement of the diffraction data at two different temperatures, T_1 and T_2. Representing the parameters by the $n \times 1$-D vectors p_{T_1} and p_{T_2}, the distance is defined as[34]

$$d_n = \left(\frac{1}{n}(p_{T_1} - p_{T_2})^T V^{-1} (p_{T_1} - p_{T_2})\right)^{1/2}$$

where V is the variance−covariance matrix of the n parameters at either T_1 or T_2 and $n = 117$ (5 quadrupole, 3 dipole, and 1 monopole for each hydrogen atom, 7 octopole, 5 quadrupole, 3 dipole, and 1 shell monopole for each carbon atom, and 1 common core monopole for all carbon atoms). If the differences between p_{T_1} and p_{T_2} reflect only random errors, d_n will be close to unity. Table 3 contains the d_n values for all combinations of temperatures and variance−covariance matrices. When the variance−covariance matrix of the higher temperature is used, the distance decreases, reflecting the fact that the variances increase with increasing temperature. The d_n values involving the 205a K data are all rather large, probably as a consequence of the higher temperature, where $(I/\sigma(I))$ ratios decrease and the anharmonic contributions to the ADPs increase, making it more difficult to obtain reliable ADPs and to deconvolute these

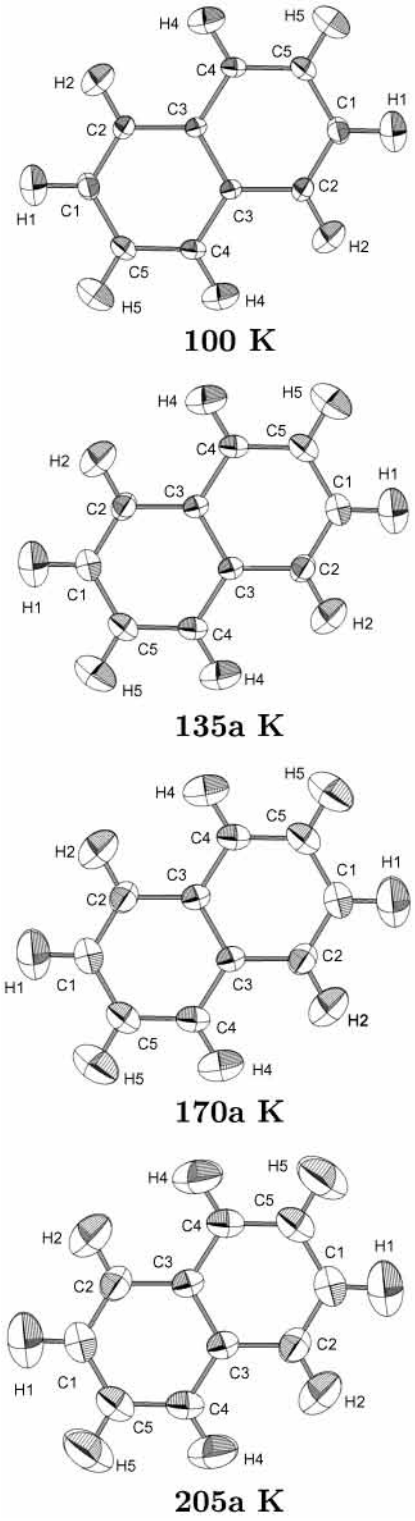

Figure 2. ORTEP[33] drawings of naphthalene at the four different temperatures showing thermal ellipsoids at the 50% probability level.

from the experimental thermally averaged electron density. The results from this analysis show that though the multipole populations exhibit some variation with temperature[43] only the 205a K parameters are significantly different from the rest. The multipole populations obtained from the 135a K and 170a K data sets are in excellent agreement, and the distances to those refined from the 100 K data are also reasonable, especially when taking into consideration that this data set was measured on a different crystal. We therefore conclude that the deconvolution

TABLE 3: Comparison of Electronic Parameters (d_n) at Different Temperatures[a]

	100 K	135a K	170a K	205a K
100 K		2.9	4.7	9.5
135a K	3.3		2.8	7.7
170a K	5.4	3.1		7.9
205a K	11.0	9.1	8.7	

[a] The variance−covariance matrix of the entry in the top row is used.

TABLE 4: Intramolecular BCPs[a]

1	2	ρ/eÅ^{-3}	$\nabla^2\rho$/eÅ^{-5}	ϵ	d1/Å	d2/Å
C(1)	C(2)	2.252(10)	−20.1(4)	0.263(17)	0.707	0.667
		2.167	−21.32	0.216	0.6869	0.6874
		2.180	−21.70	0.257	0.6872	0.6890
C(5)	C(4)	2.234(10)	−19.5(4)	0.255(16)	0.679	0.696
		2.167	−21.35	0.212	0.6900	0.6851
		-	-	-	-	-
C(1)	C(5)[b]	2.030(11)	−16.7(4)	0.185(18)	0.704	0.711
		2.003	−18.61	0.141	0.7085	0.7071
		2.029	−19.31	0.173	0.7083	0.7083
C(2)	C(3)	2.058(10)	−16.2(3)	0.198(17)	0.716	0.702
		2.016	−18.94	0.127	0.7038	0.7146
		2.019	−19.09	0.161	0.7089	0.7121
C(4)	C(3)	2.038(10)	−16.3(3)	0.201(17)	0.703	0.715
		2.023	−19.08	0.128	0.7001	0.7180
		-	-	-	-	-
C(3)	C(3)[b]	2.024(11)	−15.7(4)	0.176(18)	0.710	0.710
		2.023	−19.05	0.110	0.7103	0.7103
		1.983	−28.34	0.149	0.7168	0.7168
H(1)	C(1)	1.638(7)	−11.33(19)	0.069(9)	0.363	0.720
		1.932	−23.76	0.010	0.3970	0.6861
		1.918	−24.52	0.017	0.4073	0.6788
H(5)	C(5)	1.597(7)	−10.29(18)	0.058(9)	0.369	0.714
		1.930	−23.73	0.010	0.3965	0.6868
		-	-	-	-	-
H(2)	C(2)	1.607(7)	−10.33(18)	0.054(9)	0.366	0.717
		1.938	−23.95	0.009	0.3951	0.6882
		1.912	−24.32	0.018	0.4078	0.6792
H(4)	C(4)	1.604(7)	−10.52(19)	0.070(10)	0.372	0.712
		1.952	−24.51	0.009	0.3903	0.6929
		-	-	-	-	-

[a]First line from the experimental crystal density, second line from the periodic calculation, and third line from the isolated-molecule geometry optimization. [b] $-x, -y, -z$.

of thermal motion from the electron density has been achieved for the data measured below 200 K.

The successful deconvolution of the thermal motion from the electron density enables a comparison of the resulting static electron density with theoretical electron densities for molecular and crystalline naphthalene via a topological analysis. Because the static electron densities are identical at the three lowest temperatures, the subsequent comparison is based on a refinement of the 135a K data.

Topological Analysis of the Electron Density. Valuable information on both intra- and intermolecular interactions can be obtained from the topological analysis of the electron density, $\rho(\mathbf{r})$.[1,35] Critical points (CPs) of rank 3 were identified in the experimental and theoretical electron densities, and the (3, −1) or bond critical points (BCPs) have been investigated more closely. Atomic properties have been calculated by integration over the atomic basins (Ω) bound by the zero-flux surfaces of $\rho(\mathbf{r})$.[18,30,36]

Intramolecular Topology. The values of $\rho(\mathbf{r})$, $\nabla^2\rho(\mathbf{r})$, and ϵ at a given intramolecular BCP (Table 4) are very similar for the three static electron densities (experimental, theoretical crystal, and isolated molecule). The positions of the BCPs differ by less than 0.02/0.05 Å for the C−C/C−H bonds. The C(1)−C(2) and C(5)−C(4) bonds, which are equivalent for the isolated molecule, show more double-bond character than the other C−C bonds, in agreement with the shorter bond lengths (Table 5)

TABLE 5: Bond Lengths Corrected for Librational Motion

	100 K	135a K	170a K	205a K
C(1)−C(2)/Å	1.375	1.377	1.376	1.377
C(5)−C(4)/Å	1.376	1.378	1.376	1.378
C(1)−C(5)[a]/Å	1.419	1.419	1.417	1.419
C(2)−C(3)/Å	1.419	1.421	1.420	1.422
C(4)−C(3)/Å	1.419	1.420	1.419	1.420
C(3)−C(3)[a]/Å	1.424	1.424	1.422	1.424

[a] $-x, -y, -z$.

TABLE 6: Atomic Charges (q), Volumes (V), and Laplacians (L) Integrated over the Atomic Basins (Ω)[a]

	$q(\Omega)$/e	$V(\Omega)$/Å^3	$L(\Omega)$/eÅ^{-2}
C(1)	−0.0827	12.780	-3.29×10^{-3}
	−0.0498	12.514	5.34×10^{-4}
	0.0038	12.017	4.11×10^{-4}
C(2)	−0.0831	13.001	-1.16×10^{-2}
	−0.0285	12.571	6.49×10^{-3}
	−0.0017	11.834	4.21×10^{-3}
C(3)	−0.0269	9.416	-4.48×10^{-3}
	−0.0238	9.305	1.44×10^{-3}
	0.0096	10.072	2.21×10^{-3}
C(4)	−0.0695	11.339	-1.37×10^{-2}
	−0.0188	11.189	4.89×10^{-3}
	-	-	-
C(5)	−0.0630	12.002	-1.29×10^{-2}
	−0.0577	11.976	-3.33×10^{-3}
	-	-	-
H(1)	0.0876	6.714	-7.3×10^{-4}
	0.0347	7.144	2.90×10^{-5}
	−0.0018	7.418	-3.57×10^{-5}
H(2)	0.0898	6.685	-4.3×10^{-4}
	0.0437	7.013	-1.33×10^{-4}
	−0.0041	7.471	3.75×10^{-5}
H(4)	0.0758	5.765	-5.6×10^{-4}
	0.0626	5.927	1.05×10^{-3}
	-	-	-
H(5)	0.0773	8.401	0.8×10^{-4}
	0.0404	8.586	1.77×10^{-4}
	-	-	-

[a] First line from the experimental crystal density, second line from the periodic calculation, and third line from the isolated-molecule geometry optimization.

and higher electron densities and ellipticities at the BCPs. It was necessary to correct the C−C bond lengths for librational effects because the bonds appeared to be shorter at higher temperatures, reflecting the fact that the molecular librations increase with increasing temperature.

The charges, volumes, and Laplacians obtained by integration over the atomic basins are listed in Table 6. The integrated atomic Laplacians adopt values close to zero, as expected. The overall agreement is excellent for the atomic volumes determined from the experimental and theoretical electron densities. The atomic charges do not compare as well—the theoretical calculations provide almost neutral atoms whereas a more polarized model in agreement with chemical expectations is obtained from the experimental charge density. It should be noted that C(3), which is bonded to three carbon atoms, exhibits the smallest volume of the carbon atoms and that its charge is close to zero, consistent with the chemical environment.

Our initial IAM refinements gave rise to a C(4)−H(4) bond length significantly (0.04 Å) shorter than the other C−H bond lengths. This result was consistent for all four data sets recorded from two different crystals. Because the C(4)−H(4) bond points toward the bond between C(3) and C(4) ($-x, y + {}^1/_2, -z + ({}^1/_2)$) in an adjacent molecule and H(4) is situated only 2.60 Å from the centroid of the six-membered π-ring system containing these two atoms,[44] the apparently shorter C(4)−H(4) distance could reflect an intermolecular C(4)−H(4)$\cdots\pi$ antihydrogen bond. This assumption was further substantiated by spectroscopic measurements,[37] which revealed the blue shift in the vibrational spectrum upon crystallization that is taken as an indication of an antihydrogen bond.[38−41]

However, the decrease in the C(4)−H(4) bond length is so large that it is unlikely to be caused by a weak interaction such as a C−H$\cdots\pi$ (anti)hydrogen bond. The apparent shortening of the C(4)−H(4) bond obtained from the IAM refinements of the X-ray data could equally well reflect a variation in the electron distribution within the bond. This interpretation was supported by a recent multi-temperature neutron diffraction study[42] that showed no difference between the C−H bond lengths in the relevant temperature interval (80, 150, and 220 K). The C−H$\cdots\pi$ interaction could lead to an accumulation of the electron density toward the carbon atom in this particular bond, consistent with the observation that H(4) has higher populations of the dipole terms than the other hydrogen atoms.

To be certain that the apparent electron distribution in the C(4)−H(4) bond was not a result of poor modeling in the region of the hydrogen atoms, we carried out a refinement where only the ADPs and positional parameters for H(4) were varied in the final model. This resulted in a C(4)−H(4) bond of 1.0570 Å (135a K), ADPs very similar to those of the rigid body, and a dipole on H(4) of similar magnitude to the dipoles on the other hydrogen atoms. From this, we conclude that the electron distribution in the C(4)−H(4) bond differs from the remaining C−H bonds in crystalline naphthalene and that it can be modeled either correctly by a larger dipole population on H(4) or incorrectly by a shortening of its bond length. Because this variation seems to be caused by intermolecular interactions in the crystal, we subjected them to closer analysis.

TABLE 7: Intermolecular BCPs[a]

	1	2	ρ/eÅ^{-3}	$\nabla^2\rho$/eÅ^{-5}	ϵ	d1/Å	d2/Å
1	H(4)	C(4)[b]	0.055	0.665(3)	2.26(11)	1.158	1.660
			0.047	0.506	1.94	1.0922	1.6785
2	H(2)	H(1)[c]	0.051	0.592(4)	0.124(13)	1.154	1.185
			0.036	0.418	1.99	1.1464	1.1973
3	H(1)	H(1)[d]	0.035	0.424(3)	0.76(3)	1.310	1.310
			0.026	0.320	1.47	1.3095	1.3095
4	H(1)	H(5)[e]	0.032	0.387(2)	0.61(2)	1.276	1.362
			0.024	0.278	1.16	1.2607	1.3979
5	H(4)	H(4)[f]	0.031	0.381(2)	1.31(7)	1.414	1.414
			0.025	0.307	4.40	1.4136	1.4136
6	H(1)	C(5)[g]	0.030	0.378(2)	0.57(3)	1.325	1.720
			0.028	0.309	0.33	1.2554	1.7560
7	H(2)	H(4)[f]	0.030	0.367(2)	1.73(7)	1.415	1.434
			0.025	0.292	4.16	1.3529	1.5283
8	H(5)	C(2)[b]	0.023	0.284(2)	1.21(5)	1.379	1.874
			0.020	0.217	1.17	1.3081	1.9310
9	H(2)	C(1)[h]	0.021	0.280(2)	0.38(3)	1.392	1.749
			0.020	0.241	0.18	1.1313	1.8325
10	H(5)	H(5)[i]	0.006	0.067(1)	2.7(2)	1.715	1.715

[a] First line from the experimental crystal density and second line from the periodic calculation. [b] $-x, y + {}^1/_2, -z + {}^1/_2$. [c] $-x - 1, y + {}^1/_2, -z - {}^1/_2$. [d] $-x - 2, -y, -z - 1$. [e] $x - 2, y, z - 1$. [f] $-x, -y + 1, -z$. [g] $x - 1, -y + {}^1/_2, z - {}^1/_2$. [h] $x, -y + {}^1/_2, z + {}^1/_2$. [i] $-x + 1, -y, -z$.

Intermolecular Interactions. The intermolecular bond critical points in crystalline naphthalene are listed in Table 7 in order of decreasing $\rho(\mathbf{r})$, an indication of the strength of the corresponding intermolecular interaction, with the interaction involving the unique H(4) at the top of the list. The crystal packing in naphthalene should be determined by weak van der Waals interactions, and consistent with this, all of the intermolecular BCPs have values of $\rho(\mathbf{r})$ that are 10−25% of the value for an ordinary hydrogen bond. Despite this, we find good internal consistency between the positions and characteristics of the intermolecular BCPs from the experimental and theoretical charge densities. The BCPs connect the same atoms and

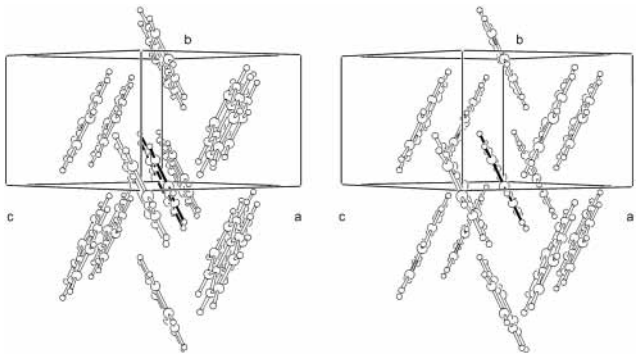

Figure 3. Stereo pair of the 12 nearest neighbors of a naphthalene molecule (filled bonds) in the crystalline state.

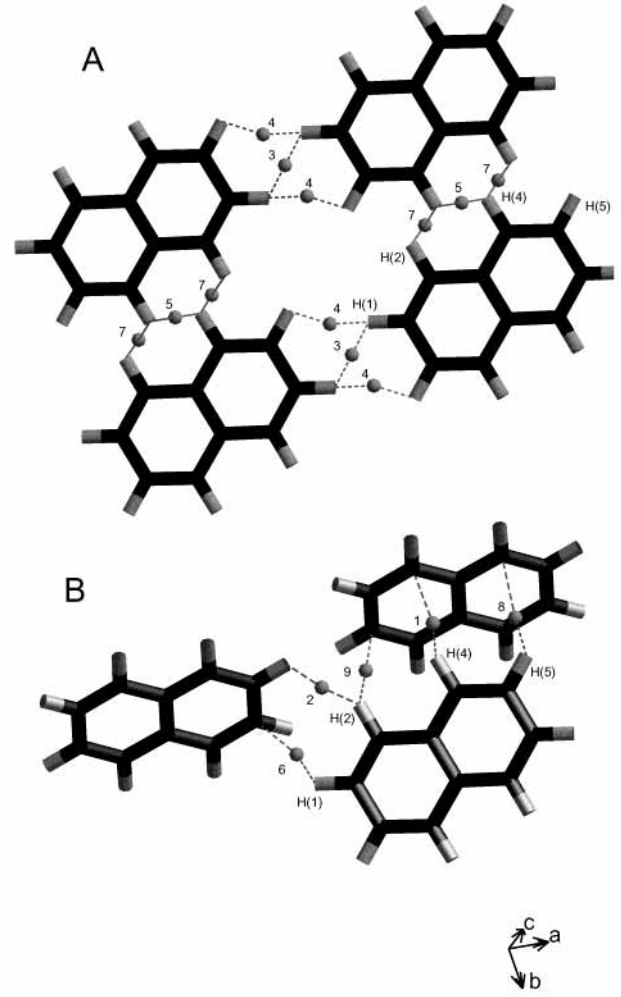

Figure 4. Illustration of the intermolecular interactions in crystalline naphthalene with the corresponding BCPs shown as spheres. (A) H···H contacts. (B) C−H···C contacts.

the positions do not vary more than 0.3 Å. The values of $\rho(\mathbf{r})$, $\nabla^2\rho(\mathbf{r})$, and especially ϵ vary slightly more than for the intramolecular BCPs, but the relative values are the same. Minor deviations are associated with critical points at special positions in the unit cell where the uncertainty in the experimental electron density is high. The ($^1/_2$), 0, 0) special position is a (3, 1) CP in the theoretical electron density, and it is a BCP of low electron density and high ellipticity, situated only 0.27 Å from an extra (3, 1) CP, in the experimental electron density.

The 12 nearest neighbors in the herringbone packing of the naphthalene molecules are shown in Figure 3. The first nine intermolecular BCPs and the corresponding gradient paths from the experimental electron density are depicted in Figure 4. It shows the two types of interactions present in the herringbone packing. H···H interactions connect molecules related by translational symmetry (Figure 4A), and molecules related by 2-fold screw axes and glide planes (Figure 4B) interact mainly through C−H···C contacts.

Because it seems likely that the special electron distribution in the C(4)−H(4) bond is caused by intermolecular interactions, the environment of H(4) was examined. The short intermolecular contact distances from H(4) combined with the finding of the intermolecular BCP of the highest electron density in this contact are consistent with the small atomic volume of H(4) (Table 6). These observations support the fact that the unique distribution in the C(4)−H(4) bond is due to an intermolecular C−H···π interaction.

Conclusions

On the basis of a new set of high-resolution X-ray diffraction data collected at multiple temperatures, we have shown that it is possible to deconvolute thermal motion and static electron density in crystalline naphthalene at temperatures below 200 K. The static crystal electron density obtained from the diffraction data is virtually identical to those obtained by theoretical calculations showing identical features of the intra- and intermolecular BCPs. The crystal packing possesses a C−H···π interaction that alters the electron distribution in the C−H bond, drawing it further toward the carbon atom and decreasing the atomic volume of the hydrogen atom.

Acknowledgment. This research was supported through grants from the Danish Natural Science Research Council. We are grateful for help from Mr. F. Hansen with the crystallographic experiments and from Dr. C. Flensburg in the analysis of the multipole parameters. We thank Professor A. Albinati, Professor T. Willis, and Dr. S. Mason for informing us about their results from a multi-temperature neutron diffraction study and A. Ø. Madsen and H. O. Sørensen for helpful discussions.

Supporting Information Available: Difference density maps, refined atomic coordinates, rigid body tensors, ADPs, and multipole parameters from the four data sets. This material is available free of charge via the Internet at http://pubs.acs.org.

References and Notes

(1) Bader, R. F. W. *Atoms in Molecules: A Quantum Theory*; Oxford University Press: New York, 1994.
(2) Coppens, P. *X-ray Charge Densities and Chemical Bonding*; Oxford University Press: New York, 1997.
(3) Abrahams, s. C.; Monteath Robertson, J.; White, J. G. *Acta Crystallogr.* **1949**, *2*, 233−235.
(4) Cruickshank, D. W. J. *Acta Crystallogr.* **1957**, 504−508.
(5) Ponomarev, V. I.; Filipenko, O. S.; Atovmyan, L. O. *Kristallografiya* **1976**, *21*, 392−394.
(6) Brock, C. P.; Dunitz, J. D. *Acta Crystallogr.* **1982**, *B38*, 2218−2228.
(7) Pawley, G. S.; Yeats, E. A. *Acta Crystallogr., Sect. B* **1969**, *25*, 2009−2013.
(8) Natkaniec, I.; Belushkin, A. V.; Dyck, W.; Fuess, H.; Zeyen, C. M. E. *Z. Kristallogr.* **1983**, *163*, 285−293.
(9) Schomaker, V.; Trueblood, K. N. *Acta Crystallogr., Sect. B* **1968**, *24*, 63−76.
(10) Brock, C. P.; Dunitz, J. D.; Hirshfeld, F. L. *Acta Crystallogr., Sect. B* **1991**, *47*, 789−797.
(11) Bürgi, H.-B.; Rangavittal, N.; Hauser, J. *Helv. Chim. Acta* **2001**, *84*, 1889−1906.
(12) Nonius B. V. *Collect* data-collection software; 1999.
(13) Wyckoff, R. W. G. *Crystal Structures*, 2nd ed.; Interscience Publishers: New York, 1965; Vol. 3, pp 160−165.
(14) Sørensen, H. O.; Larsen, S. *J. Appl. Crystallogr.* **2003**, *36*, 931−939.

(15) Duisenberg, A. J.; Schreurs, A. M. M. BIJVOET Centre for Biomolecular Research, Laboratory for Crystal and Structural Chemistry, Utrecht University, The Netherlands.

(16) Duisenberg, A. J. Reflections on Area Detectors. Ph.D. Thesis, Utrecht University, The Netherlands, 1998.

(17) Blessing, R. H. *Cryst. Rev.* **1987**, *1*, 3−58.

(18) Stewart, R. F.; Spackman, M. A.; Flensburg, C. *VALRAY User's Manual*, version 2.1; 2000.

(19) Stewart, R. F. *Acta Crystallogr., Sect. A* **1976**, *32*, 565−574.

(20) Bürgi, H.-B.; Capelli, S. C.; Goeta, A. E.; Howard, J. A. K.; Spackman, M. A.; Yufit, D. S. *Chem.—Eur. J.* **2002**, *8*, 3512−3521.

(21) Madsen, A. Ø.; Sørensen, H. O.; Flensburg, C.; Stewart, R. F.; Larsen, S. *Acta Crystallogr. Sect. A*, to be submitted for publication.

(22) Huber-Buser, E. Organic Chemistry Laboratory, Swiss Federal Institute of Technology, Zürich, Switzerland, 1988.

(23) Madsen, A. Ø.; Mason, S.; Larsen, S. *Acta Crystallogr., Sect. B* **2003**, *59*, 653−663.

(24) Hummel, W.; Hauser, J.; Bürgi, H.-B. *J. Mol. Graphics* **1990**, *8*, 214−220.

(25) Saunders, V. R.; Dovesi, R.; Roetti, C.; Causa, M.; Harrison, N. M.; Orlando, R.; Zicovich-Wilson, C. M. *CRYSTAL98 1.0 User's Manual*; 1998.

(26) Becke, A. D. *J. Chem. Phys.* **1993**, *98*, 5648−5652.

(27) Lee, C.; Yang, W.; Parr, R. G. *Phys. Rev. B* **1988**, *37*, 785−89.

(28) Hariharan, P. C.; Pople, J. A. *Theor. Chim. Acta* **1973**, *28*, 213−222.

(29) Spackman, M. A.; Mitchell, A. M. *Phys. Chem. Chem. Phys.* **2001**, *3*, 1518−1523.

(30) Gatti, C. *TOPOND98 User's Manual*; 1999.

(31) Frisch, M. J.; Trucks, G. W.; Schlegel, H. B.; Gill, P. M. W.; Johnson, B. G.; Robb, M. A.; Cheeseman, J. R.; Keith, T.; Petersson, G. A.; Montgomery, J. A.; Raghavachari, K.; Al-Laham, M. A.; Zakrzewski, V. G.; Ortiz, J. V.; Foresman, J. B.; Cioslowski, J.; Stefanov, B. B.; Nanayakkara, A.; Challacombe, M.; Peng, C. Y.; Ayala, P. Y.; Chen, W.; Wong, M. W.; Andres, J. L.; Replogle, E. S.; Gomperts, R.; Martin, R. L.; Fox, D. J.; Binkley, J. S.; Defrees, D. J.; Baker, J.; Stewart, J. P.; Head-Gordon, M.; Gonzalez, C.; Pople, J. A. *Gaussian 94*, revision E.2; Gaussian, Inc.: Pittsburgh, PA, 1995.

(32) http://www.chemistry.mcmaster.ca/aimpac/

(33) Johnson, C. K. Report ORNL.5138; Oak Ridge National Laboratory: Oak Ridge, TN, 1976.

(34) de La Fortelle, E.; Bricogne, G. *Methods in Enzymology*; Academic Press: New York, 1997; Vol. 276, pp 472−494.

(35) Popelier, P. *Atoms in Molecules: An Introduction*: Prentice Hall, New York; 1999.

(36) Flensburg, C.; Madsen, D. *Acta Crystallogr., Sect. A* **2000**, *56*, 24−28.

(37) Kjaergaard, H. G.; Henry, B. R. *J. Phys. Chem.* **1996**, *100*, 4749−4754.

(38) Hobza, P.; Špirko, V.; Selzle, H. L.; Schlag, E. W. *J. Phys. Chem. A* **1998**, *102*, 2501−2504.

(39) Cubero, E.; Oronzco, M.; Luque, F. J. *Chem. Phys. Lett.* **1999**, *310*, 445−450.

(40) Cubero, E.; Oronzco, M.; Hobza, P.; Luque, F. J. *J. Phys. Chem. A* **1999**, *103*, 6394−6401.

(41) Hobza, P.; Havlas, Z. *Chem. Rev.* **2000**, *100*, 4253−4264.

(42) Albinati, A.; Willis, T.; Mason, S. Private communication.

(43) The larger the temperature difference, the larger d_n. See also the actual values in Table 3S.

(44) The distances involved are all significantly shorter than 2.9 Å, the sum of the C and H van der Waals radii.